Polymer 50 (2009) 2172–2180

Contents lists available at ScienceDirect

Polymer

journal homepage: www.elsevier.com/locate/polymer

Phase dynamics and wetting layer formation mechanisms of pattern-directed phase separation in binary polymer mixture films with asymmetry compositions

Jia-Lin Li [a], Li-Tang Yan [a,b,**], Xu-Ming Xie [a,*]

[a] Advanced Materials Laboratory, Department of Chemical Engineering, Tsinghua University, Beijing 100084, PR China
[b] Lehrstuhl für Physikalische Chemie II, Universität Bayreuth, D-95440 Bayreuth, Germany

ARTICLE INFO

Article history:
Received 9 September 2008
Received in revised form
11 February 2009
Accepted 10 March 2009
Available online 19 March 2009

Keywords:
Pattern-directed phase separation
Wetting layer formation mechanisms
Asymmetry polymer blend

ABSTRACT

Focusing on the binary polymer mixture films under the off-critical condition, the phase dynamics and wetting layer formation mechanisms of pattern-directed phase separation are numerically investigated. The simulated results demonstrate that, for different compositions, the polymer mixtures on the strip patterned surface can exhibit various phase morphologies in the strips of the bulk, which can be used to tailor the microscopic structures of films. The evolutions of these phase structures in the strips of the bulk obey almost the same power law with an exponent of 1/3, i.e., the Lifshitz–Slyozov growth law for the films with various off-critical degrees. It is found that the wetting layer thickness near the patterned surface grows logarithmically at the initial stages, just like the wetting layer formation mechanism of the polymer mixture near the surface with an isotropic potential. This revels that only patterning the surface potential may not change the growth law of the wetting layer. The simulated results also indicate that the diffusion of the component in the direction parallel to the surface originates from the edge of the strips.

1. Introduction

The surface-directed phase separation (SDPS) has attracted much attention since Jones et al. found the "surface-directed spinodal decomposition waves" in the PEP-dPEP blend film where wave-vectors are normal to the surface and propagate into the bulk [1]. The experimental or theoretical works on this important topic have recently been reviewed by Krausch [2] and Puri et al. [3,4], respectively. These discussions mainly focused on the formation mechanisms of the wetting layer. Various wetting layer formation mechanisms were reported, such as surface potential dependant mechanism (for long-range surface potential), logarithmic law ($T - \ln t$) (for short-range surface potential), Lifshitz–Slyozov (LS) mechanism ($T - t^{1/3}$), and pure diffusion limited mechanism ($T - t^{1/2}$), where T and t denote the wetting layer thickness and the evolution time respectively. However, little work refers to the relation between these wetting layer formation mechanisms and different conditions, e.g., composition, quench depth, noise strength and surface interaction strength, etc. For instance, Puri and Binder [5] investigated the composition dependence of the wetting layer evolution, and found that, when the minority component is preferred by the surface, the growth law of the wetting layer obeys LS mechanism. However, it turns to logarithmic growth law when the majority component is preferred by the surface. The formation reason for these different growth laws was attributed to the difference of the bulk phase morphologies induced by the off-critical degrees of the compositions, which really reflects the changes of the interplay between the surface potential and the bulk chemical potential [5,18]. Employing a cell dynamical system (CDS) model, Marko discussed the dependence of the bulk phase morphology and wetting layer formation mechanism on surface potentials and noise strengths [6]. For the SDPS with off-critical condition, Brown et al. [7] found a transition of the power law exponent from 1/3 to 1/6 during the evolution of the wetting layer when the majority component is preferred by the surface, because a deep depletion layer of the majority component forms near the wetting layer which screens the material diffusion from the bulk to the wetting layer. The different quench depths also result in different wetting layer formation mechanisms with power laws of 1/3, 1/2 and logarithmic, which has been experimentally observed by Geoghegan et al. [8] and theoretically analyzed by Yan et al. [18]. Although many researches have been processed, it is necessary to find more evidence to identify the dependence of the wetting layer growth law on different internal and/or external conditions.

* Corresponding author. Tel.: +86 10 62773607.
** Corresponding author. Lehrstuhl für Physikalische Chemie II, Universität Bayreuth, D-95440 Bayreuth, Germany.
E-mail addresses: li-tang.yan@uni-bayreuth.de (L.-T. Yan), xxm-dce@mail.tsinghua.edu.cn (X.-M. Xie).

0032-3861/$ – see front matter © 2009 Elsevier Ltd. All rights reserved.
doi:10.1016/j.polymer.2009.03.014

Patterning the surface with ordered surface potentials which preferentially attract one of the two components, then the SDPS can be defined as pattern-directed phase separation (PDPS) [9,10]. The PDPS, which is of great theoretical and technological importance, can not only promote the understanding of the phase dynamics in the thin films, but also provide the practical applications in polymer-based microelectronic elements. Most experimental works for PDPS [9–15] mainly focused on the relations between the phase dynamics and the properties of the patterned surface, including the period, the selective surface potential, etc. The effects of the film thickness and the quench depth have been considered [9,10]. The kinetic pathway of PDPS has also been explored by the numerical method [16,17]. For example, employing the Cahn–Hilliard–Cook (CHC) equation, Kielhorn and Muthukumar. [16] firstly numerically simulated the phase morphology of the PDPS in the three-dimensional (3D) space, and examined the effects of surface potential on the growth law of the bulk phase domain. The phase morphology and evolution dynamics of PDPS with the critical condition have also been investigated by Yan et al. [17,18] in the real space and the reciprocal space, and the effects of the quench depth and the period of the pattern have been considered. However, the phase structures and dynamics of PDPS in the off-critical condition have not yet been investigated even up to now, which is more important in supplying the theoretical explanation for the corresponding experimental observations. Moreover, almost no attention is paid on the wetting layer formation mechanisms in PDPS, which really reflects the effect of the surface potential architecture on the formation of the wetting layer and consequently has a tight relation with the stability of the thin film in the practical application.

Thus, in the present paper we numerically simulate and analyze the phase morphology and evolution dynamics of PDPS with asymmetry compositions in 3D space on the basis of our previous works [17,18], coupling the CHC equation and the Flory–Huggins–de Gennes (FHdG) equation. The wetting layer formation mechanisms on the patterned surface are also examined. We hope that these investigations can give a more complete view on the PDPS and promote its practical application.

2. Model and numerical procedure

The traditional model to describe the binary mixture phase separation dynamics is the CHC diffusive equation [19],

$$\frac{\partial\phi}{\partial t} = M\nabla^2\frac{\delta F\{\phi(r,t)\}}{\delta\phi(r,t)} + \eta(r,t) \tag{1}$$

where $\phi(r,t)$ is the local fraction of component at point r and at time t. $\eta(r,t)$ is the thermal noise. M is the constant characterizing the self-diffusion ability. The same degree of polymerization, $N_A = N_B = N$, is set for a symmetric binary system. Hydrodynamic effect is neglected on the reasonable assumption that the early and intermediate stages should not be affected by the hydrodynamic effect [20]. In polymer mixture, the free energy, F, is given by the FHdG equation [21],

$$F(\phi) = \int_V \mathrm{d}r\left[\frac{\phi}{N}\ln(\phi) + \frac{(1-\phi)}{N}\ln(1-\phi) + \chi\phi(1-\phi) + \frac{b^2}{36\phi(1-\phi)}|\nabla\phi|^2\right] \tag{2}$$

where χ is the temperature-dependant Flory–Huggins dimensionless interaction parameter and b is the Kuhn statistical segment length. The integral is performed over the volume, V, of the sample. Puri et al. [3,22] deduced the two boundary conditions, which is given by Eqs. (3) and (4),

$$\frac{\partial\phi(x,z_0,\tau)}{\partial\tau} = -h_1 - g\phi(x,z_0,\tau) + \gamma\frac{\partial\phi(x,z,\tau)}{\partial z}\bigg|_{z=z_0} \tag{3}$$

$$\Delta J|_{x=z_0} = 0 \tag{4}$$

where h_1, g and γ are three parameters characterizing the static surface diagram. z_0 is the location of the surface. J is defined as the polymer flux, $J = \nabla\delta F/\delta\phi$, which is used to ensure that the flux of polymer components through the surface boundary is zero and then enforces conservation of the order parameter. It has been proved that the calculated results are more precise if Eq. (3) is coupled into the dynamic model [23]. Thus, by lumping together Equations (1)–(3), and by rescaling into a dimensionless form, the dynamic equation can be obtained as Eq. (5) [17],

$$\frac{\partial\phi(\bar{r},\tau)}{\partial\tau} = \frac{1}{2}\nabla^2\left[\frac{\chi_c}{2(\chi_f-\chi_s)}\ln\frac{\phi}{1-\phi} - \frac{2\chi}{\chi_f-\chi_s}\phi + \frac{1-2\phi}{36\phi^2(1-\phi)^2}(\nabla\phi)^2 - \frac{1}{18\phi(1-\phi)}\nabla^2\phi + \left(-h_1 - g\phi + \gamma\frac{\partial\phi}{\partial z}\bigg|_{z=z_0}\right)\delta(z)\right] \tag{5}$$

Here χ_s is the spinodal value of χ at $\phi=\phi_0$, i.e., $\chi_s = 1/[2N\phi_0(1-\phi_0)]$, where ϕ_0 is the initial average concentration of component A, with $\phi_0 = 0.5$ for the critical condition in the present simulations. χ_f is the deepest quench. $\bar{r}$ and τ are rescaled spatial and temporal variables respectively, given by $\bar{r} = (|\chi_f-\chi_s|)^{1/2}r/l$ and $\tau = NM(\chi_f-\chi_s)^2t/l^2$. $\delta(x)$ is the Dirac-delta function, ensuring that the surface free energy only affects $z_0 = 1$.

Eq. (5) can be solved using the finite difference approach [24]. Numerically, for the sake of numerical stability and higher accuracy, the Laplacian ∇^2 is discretized based on the cell dynamics scheme (CDS) proposed by Oono and Puri [25]. It is then transformed as,

$$\nabla^2 X \to \frac{1}{\xi^2}(\langle\langle X\rangle\rangle - X) \tag{6}$$

where ξ is the cell size. $\langle\langle X(\bar{r},\tau)\rangle\rangle$ represents the following summation of $X(\bar{r})$ for the nearest neighbors $(\bar{r}\cdot)$ and the next-nearest neighbors $(\bar{r}\cdot\bar{r}\cdot)$, and the next–next-nearest neighbors $(\bar{r}\cdot\bar{r}\cdot\bar{r}\cdot)$:

$$\langle\langle X(\bar{r})\rangle\rangle = B_1\sum_{\bar{r}=\bar{r}\cdot}X(\bar{r}) + B_2\sum_{\bar{r}=\bar{r}\cdot\bar{r}\cdot}X(\bar{r}) + B_3\sum_{\bar{r}=\bar{r}\cdot\bar{r}\cdot\bar{r}\cdot}X(\bar{r}) \tag{7}$$

where B_1, B_2, and B_3 are 6/80, 3/80 and 1/80 for the 3D system. In order to avoid the discretization effect due to the lattice size [23], the surface terms h_1, g and γ are rescaled by the step length of the spatial discretization, $\Delta\bar{r}$, and are listed as follow,

$$h_1 \to h_1/\Delta\bar{r};\quad g\to g/\Delta\bar{r};\quad \gamma\to\gamma/\Delta\bar{r} \tag{8}$$

The simulation is carried out in the similar conditions as the previous work [17], The free boundary conditions were applied at the other end in the z-direction, and periodic boundary conditions were applied in x and y directions. The thickness of the film is fixed at 16, and the periodicity of the stripe patterned surface is denoted by $\lambda = 16$. Noise, with the magnitude of $\pm1\times10^{-3}$, was only added once at the start of the quench. The interaction strengths of the surface potential, h_1, of the blue and red strips in this figure were set 0.5 and −0.5

respectively. $g = 0.1$, $\gamma = 0.1$ and $N = 200$ were set in all simulations. To simplify the numerical procedure, and to avoid having to rescale the lattice, $\chi_f - \chi_s$ was chosen to be the same before and after the quench, and was fixed at 0.0133 throughout simulations. A dimensionless parameter, ε, which is defined as $\varepsilon = (\chi - \chi_c)/\chi_c$, denotes the quench depth in this work, and $\varepsilon = 0.1$ was set for all simulations. The Δt(time step) value used during the temporal discretization was 1×10^{-4}, and the spatial discretization step was $\Delta\bar{r} = 0.5$. Various calculations with compositions of 0.3, 0.35, 0.4, 0.45, 0.5, and 0.6 were carried out to examine the effects of the composition.

3. Results and discussions

In this section, the 3D phase morphologies during evolution are firstly introduced. Then, the evolution dynamics of the phase structures in the bulk is investigated in the reciprocal space by two-dimensional Fourier Transformation (2DFT). The wetting layer formation mechanisms are discussed by contrasting different growth laws observed in the films with different compositions.

3.1. Phase morphologies and phase inversion

The 3D morphologies' evolution of the films on a strip patterned surface with the time increasing from 0 to 1000 is illustrated in Fig. 1.

The concentration of the preferential component, i.e., component A, is marked with the color bar in the 3D figure. It can be found from Fig. 1 that the ordered phase structures induced by the strip pattern originally occur near the surface, and then penetrate into the bulk gradually. The penetrating speeds of the anisotropic waves induced by the patterned surface vary with the change of compositions. Correspondingly, the phase structures in the polymer/air interface exhibit different morphologies. The nearer the composition is away from the critical point ($\phi = 0.5$), the faster the surface

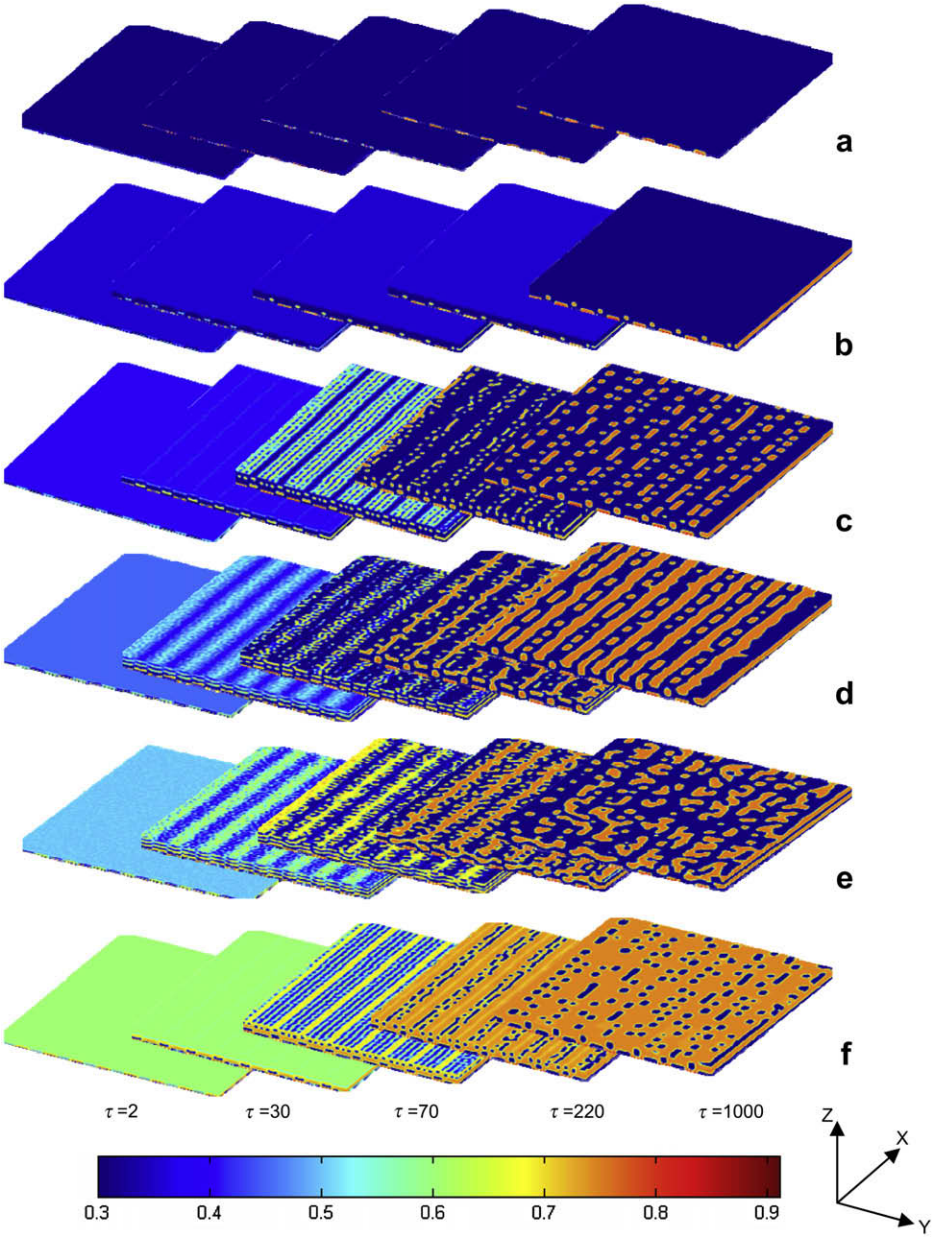

Fig. 1. 3D patterns showing the morphology evolutions of different compositions, the color bar indicates the concentration of component A. $\phi = 0.3$ (a), 0.35 (b), 0.4 (c), 0.45 (d), 0.5 (e) and 0.6 (f). [For interpretation of color referred in this figure legend the reader is referred to web version of the article.]

effect propagates into the bulk and the clearer the strip pattern can be seen in the polymer/air interfaces. For the mixtures with compositions 0.3 and 0.35, the phase separation is mainly induced by the wavelength of the patterned surface.

From the lateral direction, the checkerboard-like structures [10,17] also appeared during the dynamical evolution of the phase structures (Fig. 1(c)–(f)). In the late stages, the checkerboard-like structures finally coarsen to cylindrical (Fig. 1(c), (d), (f)) or bi-continuous (Fig. 1(e)) structures due to the effects of the stronger bulk phase separation [16,17]. Comparing Fig. 1(c) with (f), one can find that the phase structures in these two cases are almost the same because the compositions of the preferential component for the strips with different potentials are the same in these two cases ($\phi = 0.4$ and $\phi = 0.6$). Clearly, these two symmetric situations have almost the same evolution dynamics. Thus, in the following discussion, we would like to focus on the phase evolution dynamics and the wetting layer formation mechanisms with compositions $\phi = 0.35$–0.5.

Fig. 2 shows the phase morphologies in the polymer/air interface ($z = 16$). The patterns with compositions $\phi = 0.35$, 0.4, 0.45 and 0.5 are listed from top to bottom, and the time from left to right are 30, 70, 220 and 1000 respectively.

It is obvious that the phase inversion, where A-rich phases will transform to B-rich ones, occurs during the phase evolution except that the mixture with $\phi = 0.35$ does not undergo phase separation due to the high off-critical degree [5,18]. The branch structures at the boundary between two close stripes can be observed in Fig. 2(b)–(d), demonstrating that the inversion of the phase morphology from in-phase to out-of-phase originates from the edges of the strips [10,17]. The mixture with $\phi = 0.4$ is selected as an example to gain detailed insight into this inversion especially near the patterned surface.

The evolution of the morphologies (Fig. 3(b)) and the concentration profiles at the layer with $z = 2$ (Fig. 3(c)) are illustrated. As shown in Fig. 3(a), for convenience, only a small region of one certain strip is considered. It is described in Fig. 3(b) that the inversion of the preferential component starts from the edge of the middle strip, and diffuses gradually to its close strips. Finally, the middle strip is dominated by the inversed component, demonstrating that a phase inversion occurs in this strip.

Fig 3(c) plots the averaged concentration, ϕ_{av}, along y axis, which indicates the concentration fluctuation during the phase evolution [17]. At the initial stage ($\tau = 2$), the concentrations of component A in the A-preferring strips ($y = 0$–8, 16–24, 32–40,…) are lower than the average concentration, i.e., $\phi = 0.40$, which is due to the z-direction diffusion of component A towards the wetting layer due to the attraction from the surface. This mechanism is similar to that of general SDPS [1–8]. However, at the edge of each stripe, the situation differs. One can note that the concentration in the edge extremely increases, leading to a strong fluctuation. Basically, the concentration fluctuation is induced by the difference of the potentials of the close strips. Then, the component

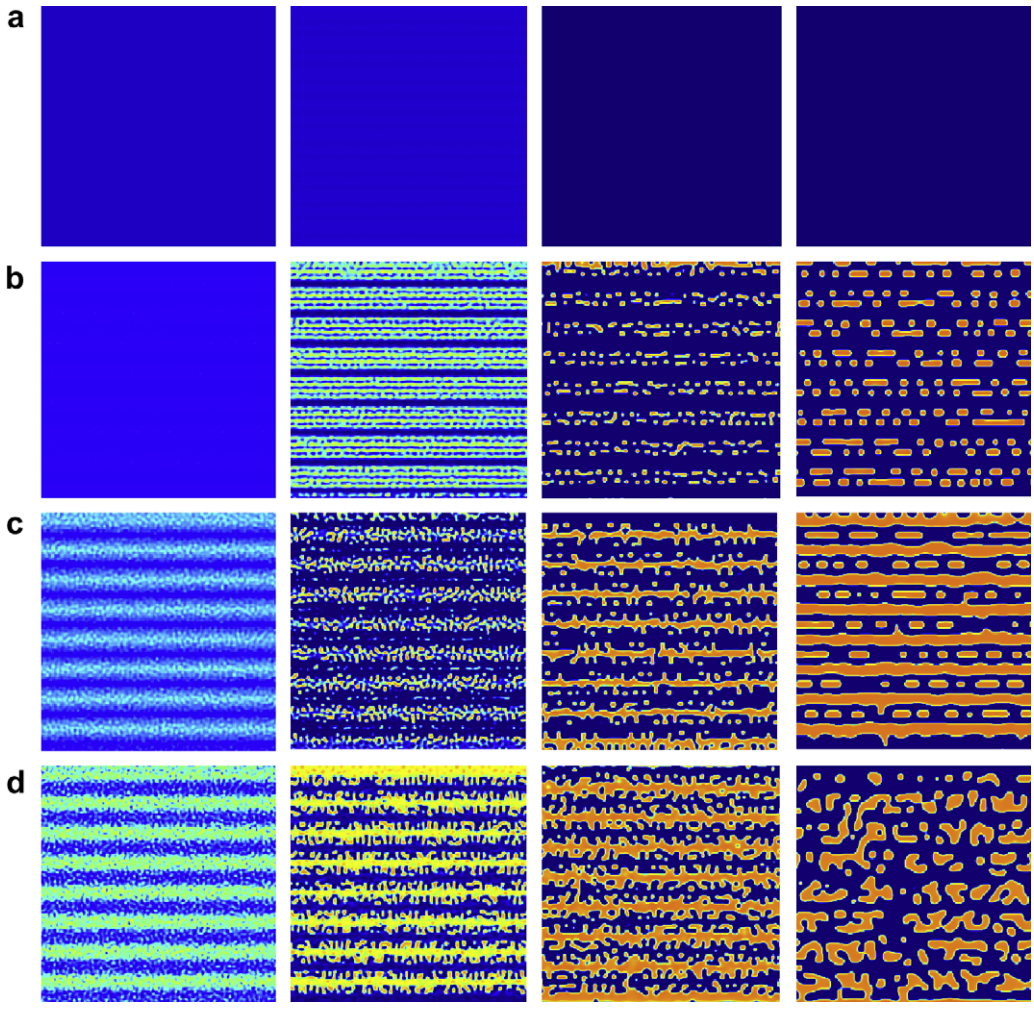

Fig. 2. 2D morphologies in polymer/air interface with different compositions. From left to right: $\tau = 30$, 70, 220 and 1000.

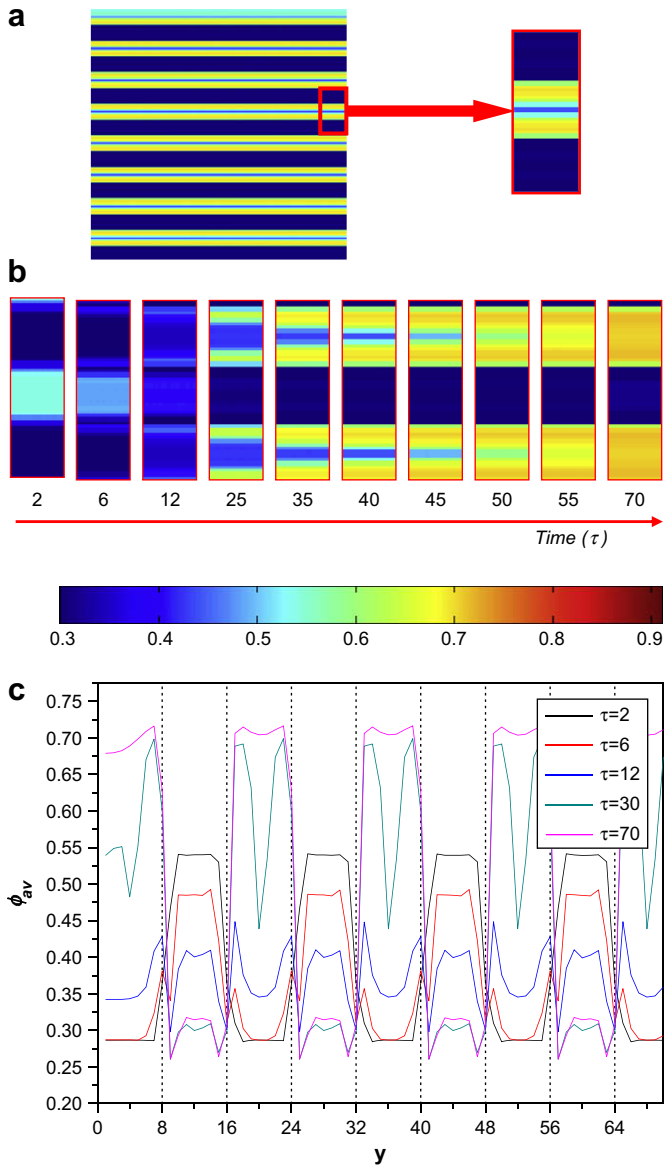

Fig. 3. Phase morphologies and evolution at the layer with $z=2$ and $\phi=0.4$. (a) Schematic diagram showing the region used for analysis. (b) Phase evolution at the layer with $z=2$. (c) Plots of the averaged concentration profiles along y axis with the increasing time.

accumulating in the fluctuation waves near the edges diffuses to the middle of the close trips until the concentration at the edges between two close strips is uniform ($\tau=70$). Thus, the diffusion of the component parallel to the surface originates from the edge of the strips, corresponding to the illustration of Fig. 3(b). Moreover, the component diffusions in both z and y directions are observed in the present study, which enriches our previous works [17].

3.2. Analysis of kinetic pathway in the reciprocal space

The pattern in the real space can be transformed into that in the reciprocal space by 2DFT. Fig. 4 is an example showing this transformation for the pattern in the polymer/air interface.

As shown in Fig. 4, the 2DFT image is characterized by two features [9,10,14]: a diffusive ring and a series of sharp harmonic peaks uniformly distributed along the vertical axis. According to the discussion in our previous work [17], the amplitudes of the harmonic peaks will fluctuate with the increasing time, corresponding to the phase inversion among the strips. Thus, from the pattern in the reciprocal space, both the isotropic phase structures in the strips and the anisotropic periodic structures can be investigated separately.

Fig. 5 illustrates the temporal evolution of the amplitudes for the first harmonic peaks in the anisotropic period profiles (Fig. 4(c) bottom) with various compositions. The amplitude of the first harmonic peak (J_1) reflects the status of the corresponding period structure very well [17]. In general, the larger J_1 is, the more obvious the first order period structure is. It is obvious in Fig. 5 that the $\phi=0.45$ sample has the largest amplitude which fluctuates within a longer time range. Thus, a higher off-critical composition corresponds to a narrower range for the phase inversion. Moreover, it is also obtained that the phase separation in the polymer/air interface is less influenced by the surface with higher off-critical degree, consistent with the previous discussions.

3.3. Wetting layer formation mechanisms

In this section the wetting layer formation mechanism of PDPS is discussed, which, as far as we know, has not yet been reported elsewhere. Actually, the formation of wetting layer near a patterned surface reflects the effects of the surface potential architecture on the phase separation and consequently closely relates to the stability of the thin film in the practical application. To define the wetting layer thickness, we firstly introduce a parameter, $P(z,\tau)$, which can be defined as follows [26]:

$$P(z,\tau) = \sum_{x,y} \frac{\phi(x,y,z,\tau)\sigma(x,y)}{L^2|\phi(x,y,z,\tau)|} \tag{9}$$

where L is the side size of $x-y$ plane. $\sigma(x,y)$ describes the preassigned pattern on the surface, and $\sigma(x,y)=1$, -1 respectively denotes A, B preferring element of the surface. If the domain morphology at plane z and at time τ is perfectly in-phase, $P(z,\tau)=1$, while $P(z,\tau)=-1$ if the morphology is totally out-of-phase. Any intermediate value of $P(z,\tau)$ $(-1<P(z,\tau)<1)$ would correspond to a domain morphology between these two extremes.

Fig. 6 shows the plots of P against z with time evolution for various compositions.

According to the $P-z$ profiles, the concentration fluctuation induced by the substrate occurs near the substrate originally, and then penetrates into the bulk. When the composition is 0.35 or 0.30, far away from the critical point, the surface effect only affects the system near the substrate, and plays little role on the phase separation of the polymer/air interface, which agrees with the above discussions. For the composition near the critical point, the surface effect can however influence the bulk phase separation to a certain extent, leading to the phase inversion in the bulk.

In the present study, the wetting layer thickness is defined as the z value when P firstly reaches zero along z-direction. The evolution dynamics of the wetting layer can be examined by plotting the wetting layer thickness against the evolution time. Fig. 7 illustrates the wetting layer thickness as functions of evolution time for various compositions at the initial stage. Actually, a longer calculation may be needed to determine the wetting layer formation mechanisms at the later stage, which needs too much calculation energy. In the practical application, a very short evolution time is usually necessary for obtaining an ordered microscopic structure in the polymer/air interface, because the ordered structures induced by the patterned surface will be destroyed at the later stage due to the increasing phase morphology evolution in the bulk [9,10,17]. In an acceptable range, it can be found from Fig. 7 that the

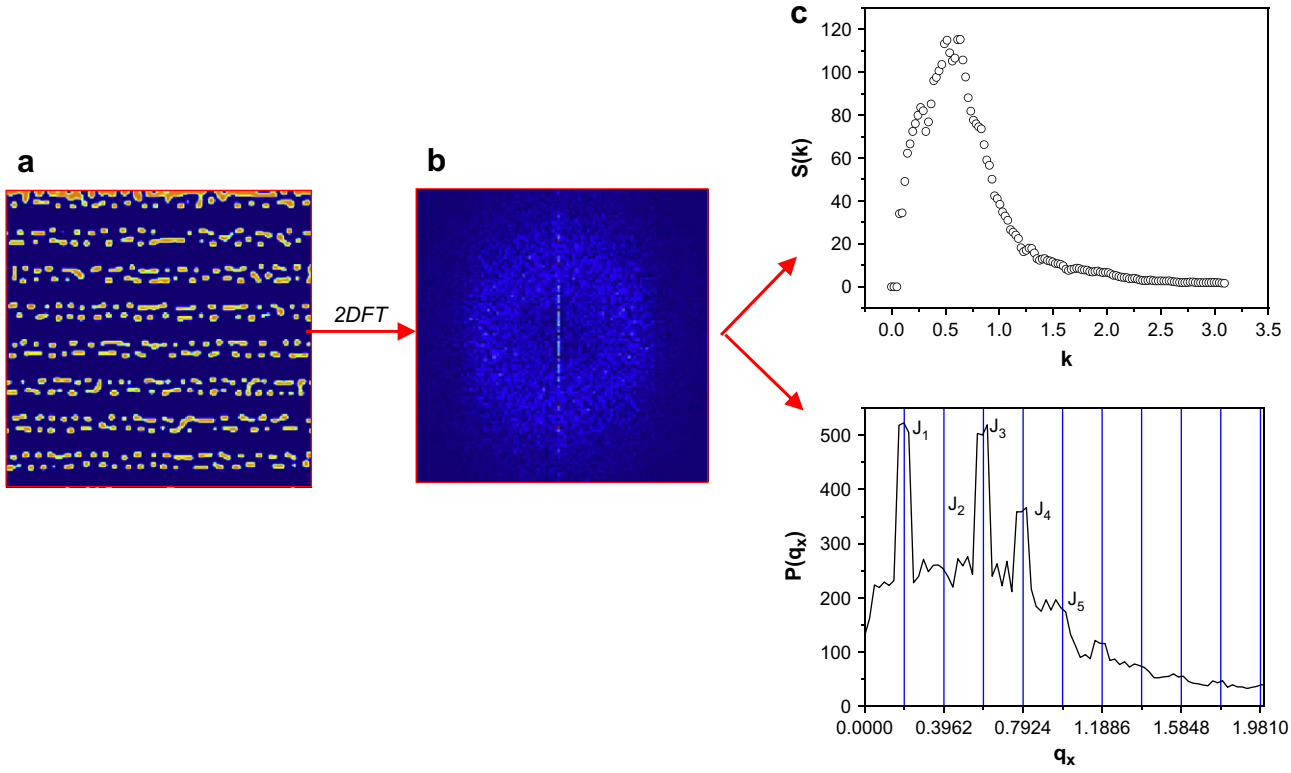

Fig. 4. The schematic diagram showing the analysis process in the reciprocal space. (a) 2D morphology in the real space, (b) the spectrums of the structure factor, (c) Top: isotropic component, bottom: anisotropic component where J_n ($n = 1, 2, 3, 4, 5$) denotes the intensity of each peak in the anisotropic spectrum.

evolution of the wetting layer obeys the power law, $T - \ln(\tau)$, which is the logarithmic mechanism. The simulated results of SDPS with a uniform surface potential demonstrate that the wetting layer formation mechanisms at the initial stage are determined by the forms of the surface potential, i.e., the long-range surface potential or the short-range surface potential [3–5,18,22]. Generally speaking, a long-range surface potential corresponds to a surface potential dependant mechanism while a short-range surface potential leads to a logarithmical growth law of the wetting layer [4,18,22]. As shown in Eq. (3), the form of the surface potential used in the present study is really the short-range potential [18,22]. Thus, the wetting layer thickness grows logarithmically at the initial time. This also reveals that only patterning the surface potential may not change the growth law of the wetting layer.

The logarithmical growth law can be understood as follow. In a viewpoint of polymer morphology, the phase separation comes to being in the bulk although the degree of the phase separation is very shallow in this stage. As shown in the schematic diagram in Fig. 7, the interface between the wetting layer and the bulk is very flat. Thus, the wetting layer formation mechanism only obeys logarithmical growth law in this stage [2,8,18]. This mechanism can also be obtained by dynamical scaling analysis, which can be found in our previous work regarding the SDPS system [18]. As a matter of fact, the nature of the phenomena why the evolution of the wetting layer exhibits different mechanisms is due to the interaction between the surface potential and the chemical potential in the bulk [5,18].

3.4. Evolution dynamics

In the reciprocal space analysis of 2DFT, the character size of the phase domains can be represented by k^* where the structure factor $S(k^*)$ reaches its maximum. In the present simulation, k^* is obtained by fitting the $S(k^*) - k^*$ curve with the Lorentz equation, $S(k) = a + b/[(k - k^*)^2 + c]$ [9,10,17].

Fig. 8 plots k^* against evolution time for various compositions in a log–log scale. The linear fit for the data indicates that the evolution dynamics of the isotropic phase separation in the strips of the bulk obeys the 1/3 power law ($k^* - \tau^{1/3}$), i.e., the LS mechanism (Fig. 8(a) and (b)), except for $\phi = 0.35$ (Fig. 8(c)) which does not undergo any phase separation in the bulk as discussed above. However, the kinetic mechanism may exhibit diffusion limited growth law ($k^* - \tau^{1/2}$) [27] or logarithmic growth law ($k^* \sim \ln(\tau)$)

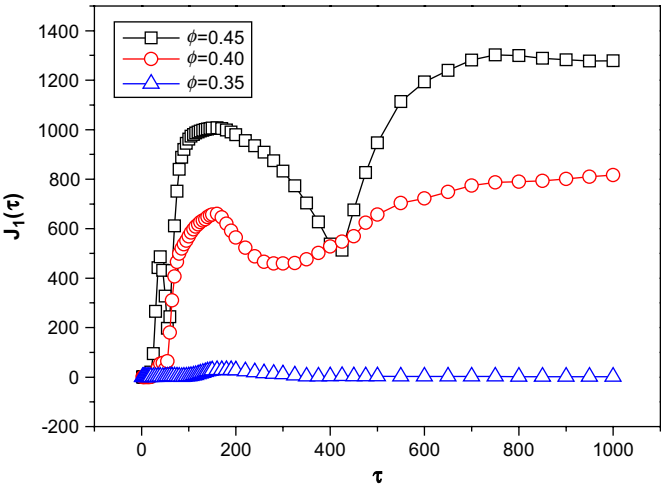

Fig. 5. The temporal evolution of the amplitudes for the first harmonic peaks in the anisotropic period profiles (Fig. 4(c) bottom) with different compositions.

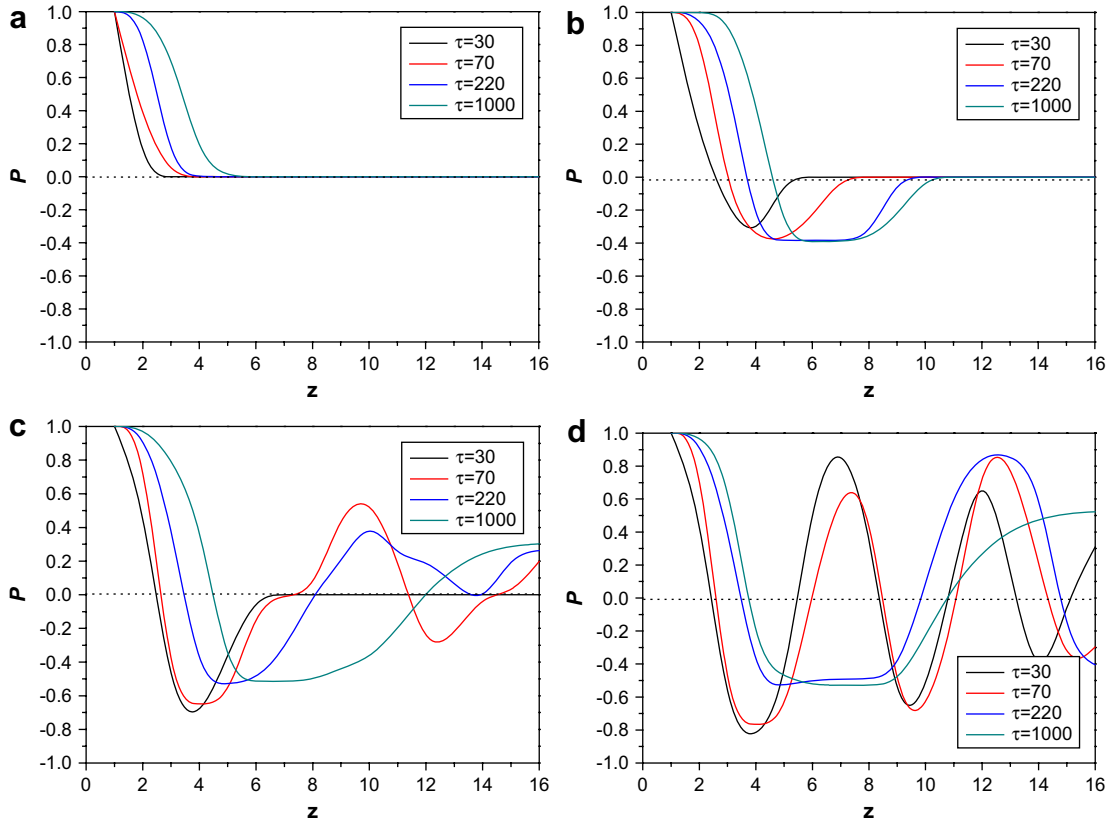

Fig. 6. The parameter, P, as functions of z at different times for various compositions. $\phi = 0.3$ (a), 0.35 (b), 0.4 (c) and 0.45 (d).

[28] for a very thin film, where the surface potential is a majority effect factor.

It is necessary to point out that, there are respectively two platforms in the dynamic curves of Fig. 8(a) and (b), which is marked by A, B, C and D. To understand the cause of the platforms in Fig. 8, the concentration profiles' ($P-z$) evolution of $\phi = 0.45$ sample is plotted, separated by A/B points (Fig. 8(d)–(f)). For example, Fig. 8(d) is the concentration profiles from $\tau = 100$ to $\tau = 240$ ($A'A$), while Fig. 8(e) from $\tau = 240$ to $\tau = 650$ (AB), Fig. 8(f) from $\tau = 650$ to $\tau = 1000$ (BB').

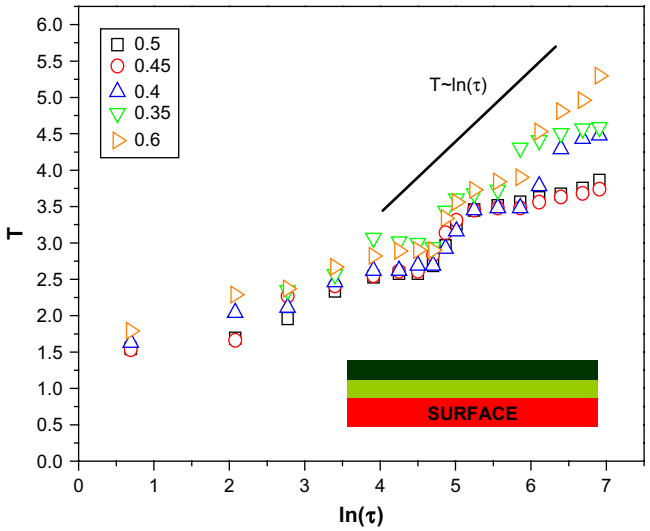

Fig. 7. The wetting layer thickness as functions of logarithmical evolution time. The schematic diagram indicates the morphology of the wetting layer thickness, where the colors of red, shallow green and deep green denote the surface, the wetting layer and the depletion layer respectively. [For interpretation of color referred in this figure legend the reader is referred to web version of the article.]

From Fig. 8(d)–(e), the difference of dynamics among periods $A'A$, AB and BB' can be examined. On the basis of the former discussion, the phase separation on the surface is affected by the concentration fluctuation oriented from the substrate. The change of concentration profiles with time indicates the transfer of substrate effect, which provides the driving force for the molecule diffusion in z-direction. During period $A'A$ (Fig. 8(d)), it is obvious that, the diffusion occurs between the central peak and trough of the $P-z$ profile fluctuation, according to the direction marked in the figure. Then, the concentration profile changes from three peaks to two, and the diffusion in the period of AB occurs between the right hand side peak and the valley (Fig. 8(e)), which demonstrates that the phase separation dynamics of $A'A$ and AB separately obeys the 1/3 law, but with a little breakpoint at A, which is the first platform in Fig. 8(a).

The situation is a little different after point B, which is plotted in Fig. 8(f). No obvious change of profile can be observed from $\tau = 650$ to $\tau = 1000$, but the P value of the polymer/air surface is fixed at 0.5, indicating that the concentration of the surface comes to 0.61 (on the preferred strips) and 0.29 (on the other trips). In this situation, it is possible for the self-driving decomposition taking place on the A-preferred strips, also with the dynamics consistent with 1/3 power law. The boundary of period AB and period BB' is another platform on Fig. 8(a), i.e., platform B. The above descriptions Fig. 8(a) can also be used to explain Fig. 8(b).

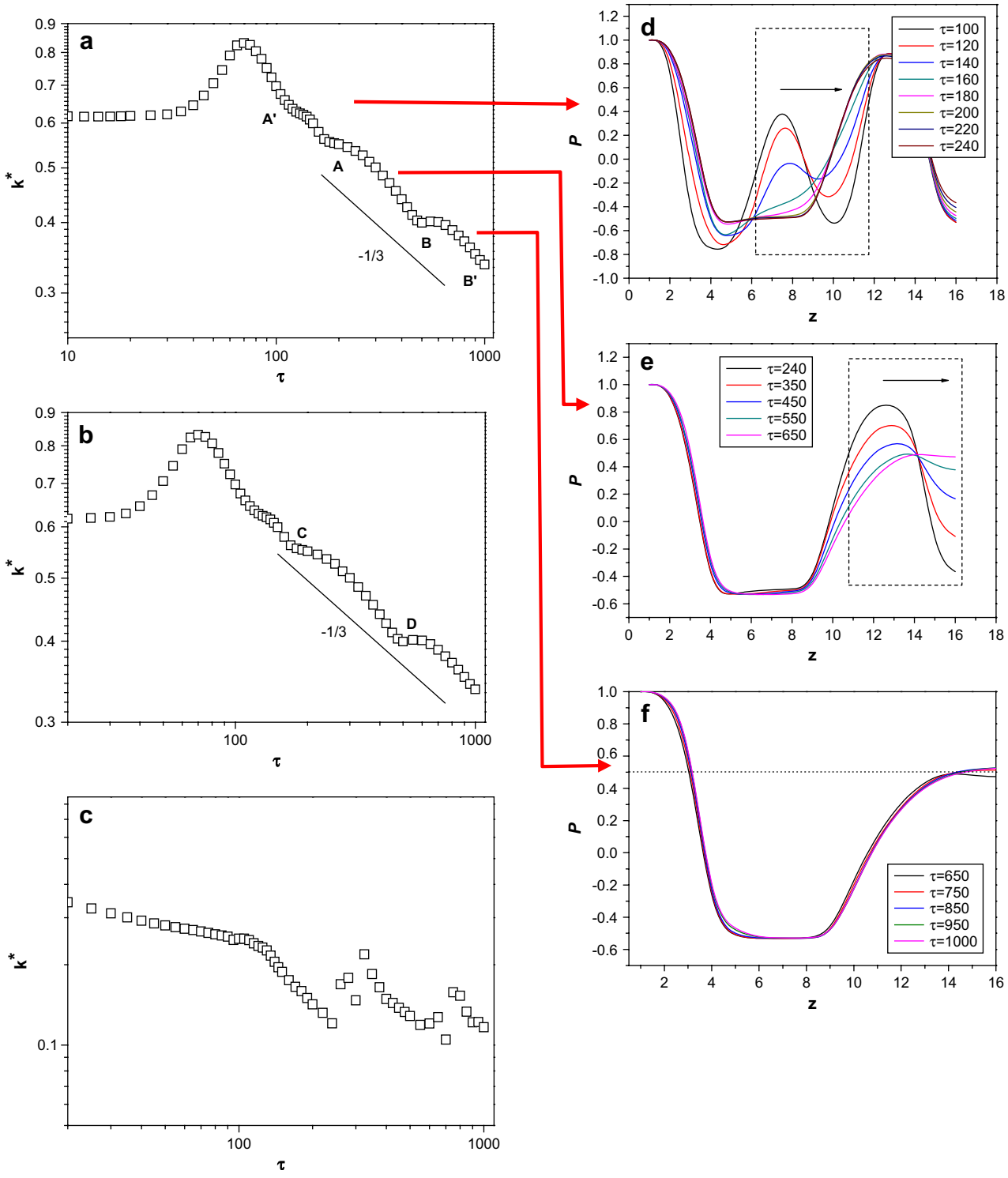

Fig. 8. $k^* - \tau$ plots for different compositions. $\phi = 0.45$ (a), 0.4 (b) and 0.35 (c), and the concentration profiles at different times for $\phi = 0.45$ (d–f).

4. Conclusion

In this paper, the PDPS has been investigated in the cases of various off-critical compositions. The simulated results demonstrate that, for different compositions, the polymer mixtures on the strip patterned surface can exhibit various phase morphologies in the strips of the bulk, which can be used to tailor the microscopic structures of films. The evolutions of these phase structures in the strips of the bulk obey almost the same power law with an exponent of 1/3, i.e., the Lifshitz–Slyozov growth law for the thick films with various off-critical degrees. It is found that the wetting layer thickness near the patterned surface grows logarithmically at the initial stages, just like the wetting layer formation mechanism of the polymer mixture near the surface with an isotropic potential. This revels that only patterning the surface potential may not change the growth law of the wetting layer. The simulated results also indicate that the diffusion of the component in the direction parallel to the surface originates from the edge of the strips. These

results can give a more complete view on the pattern-directed phase separation and promote its practical application.

Acknowledgement

Financial support from the National Natural Science Foundation of China (No. 20874056) is highly appreciated. L.-T. Yan acknowledges Alexander von Humboldt Foundation for support.

References

[1] Jones R, Norton L, Kramer EJ, Bates FS, Wiltzius P. Phys Rev Lett 1991;66:1326.
[2] Krausch G. Mater Sci Eng Rep 1995:R141.
[3] Puri S, Frisch J. Phys Condens Matter 1997;9:2109–33.
[4] Puri SJ. Phys Condens Matter 2005;17:R101–42.
[5] Puri S, Binder K. Phys Rev E 2002;66:061602.
[6] Marko JF. Phys Rev E 1993;48:2861.
[7] Brown G, Chakrabarti A, Marko JF. Phys Rev E 1994;50:1674.
[8] Geoghegan M, Ermer H, Jüngst G, Krausch G, Brenn R. Phys Rev E 2000;62:940–50.
[9] Ermi BD, Nisato G, Douglas JF, Rogers JA, Kramer A. Phys Rev Lett 1998;81:3900.
[10] Nisato G, Ermi BD, Douglas JF, Kramer A. Macromolecules 1999;32:2356.
[11] Krausch G, Kramer EJ, Rafailovich MH, Sokolov J. Appl Phys Lett 1994;64:2655.
[12] Rockford L, Liu Y, Mansky P, Russell TP, Yoon M, Mochrie SG. Phys Rev Lett 1999;82:2602.
[13] Fukunaga K, Elbs H, Krausch G. Langmuir 2000;16:3474.
[14] Li X, Xing R, Zhang Y, Han Y, An L. Polymer 2004;45:1637.
[15] Raczkowska J, Bernasik A, Budkowski A, Gao B, Lieberman M. Macromolecules 2007;40:2120.
[16] Kielhorn L, Muthukumar MJ. Chem Phys 1999;111:2259.
[17] Yan LT, Li J, Li Y, Xie XM. Macromolecules 2008;41(10):3605–12.
[18] (a) Yan LT, Xie XM. J Chem Phys 2007;126:064908;
(b) Yan LT, Xie XM. Macromolecules 2006;39:2388.
[19] (a) Cahn JW, Hilliard JE. J Chem Phys 1958;28:258;
(b) Cahn JW. J Chem Phys 1965;42:93;
(c) Cook HE. Acta Metall 1970;18:297.
[20] Siggia ED. Phys Rev A 1979;20:595.
[21] (a) Flory PJ. Principles of polymer chemistry. Ithaca, New York: Cornell University Press; 1953;
(b) de Gennes PG. J Chem Phys 1980;72:4756.
[22] Puri S, Binder K. Phys Rev A 1992;46:R4487; Phys Rev E 1992;49:5359.
[23] (a) Henderson IC, Clarke N. Macromolecules 2004;37:1952;
(b) Henderson IC, Clarke N. Macromol Theor Simul 2005;14:435.
[24] Glotzer SC. Annu Rev Comput Phys 1995;2:1.
[25] (a) Oono Y, Puri S. Phys Rev A 1988;38:434;
(b) Puri S, Oono Y. Phys Rev A 1988;38:1542.
[26] Chen H, Chakrabarti AJ. Chem Phys 1998;108:6897.
[27] Sung L, Karim A, Douglas JF, Han CC. Phys Rev Lett 1996;76:4368.
[28] Liao Y, Su Z, Ye X, Li Y, You J, Shi T, et al. Macromolecules 2005;38:211.